Estimation of crack growth on rails under the combined influence of thermo-mechanical loading due to the sliding of wheel

Aakash D Bansal*, Atul Kumar Agrawal, Vikas Rastogi

Mechanical Engineering Department, Delhi Technological University, Delhi, 110042, India.

*Email: aakashdbansal17@gmail.com; Corresponding Author.

ABSTRACT

Development and growth of surface and subsurface cracks on rail profile is one of the major reasons for deterioration of rails near the halting zones. Rail tracks are subjected to combination of thermal loads during the sliding motion of the wheel while braking and structural load due to the weight of the vehicle. In this paper, an FEA model is been developed to study and analyze the effect of coupled thermo-mechanical load during braking on contact stress and contact area at the rail-wheel interface. Both elastic and elasto-plastic FEA models are used and compared with analytical Hertzian approach to accurately predict rail-wheel contact parameters. A synthetic loading spectrum is proposed to simulate the combination of thermal and thermo-mechanical loading cycles on the rail during braking of vehicle. The loading cycle is used to predict the growth of previously present flaws using Modified Paris Law and Generalized Frost-Dugdale approach. It has been found that elasto-plastic FEA is inclined to predict lesser contact stresses than the elastic FEA or Hertzian model. Furthermore, shape of the contact patch for elasto-plastic FEA is observed to be unsymmetrical in the rolling direction unlike the elliptical contact area in elastic FEA approach. Macro scale initial cracks having length more than 2 mm are also realized to grow faster than their smaller counterparts under the combined effect of thermal and mechanical loads.

Key words: Contact Mechanics; Finite Element Modeling; Hertz contact; Stop Braking; Abaqus; Dynamic-Explicit; Plasticity.

INTRODUCTION

Railways is the most popular means of transportation and is recognized for its cost effectiveness and ride comfort when compared with other means of transportation. However, wear and damage of rails can substantially influence the service life and passenger's comfort. Rails have a service life of 8-10 years and are typically condemned due to worn out profiles. Altering of rail profile is impacted by the heat produced at the rail-wheel interface during the motion of wheel over the rail. In addition to it, the contact pressure due to the vertical load acting from the wagon contributes significantly to the wear and life of rails.

Thermal loading may result on the wheel surface from the application of the brakes. This temperature on the wheel in further addition to the heat generated due to the friction between the contacting bodies is conducted to the rail surface. The localized interaction at the contacting surface can be additionally complicated by the continuous variation in interface pressure distribution, heat generation, temperature and wear at the contact surface.

The effect of temperature and rolling contact of the wheel on the rail have been studied separately by authors previously. Taciroglu et. al. suggests that degradation of track components occurs over time due to repeated rail-wheel contact. The problem of contact in rail-wheel application is mostly addressed either analytically or by numerical methods. The analytical approach to solve rail-wheel contact can be typically categorized into: i) Normal contact problem and ii) Tangential contact. Various contact models in the above two categories have been developed over the years to successfully estimate contact stresses, size of contact patch and creepages. The class of Contact Models which assumes the surfaces in contact to exhibit elastic behavior only along with smooth contact and no friction in between the contacting surfaces comes under the category of Hertzian Models. These Hertzian Models have later evolved into Semi- Hertzian (Ayasse et. al. 2005}, Multi- Hertzian (Piotrowski et. al., 2005) or Non- Hertzian Approaches (Kalker et. al., 1993) but none of them can match the

relative ease of computation of contact parameters offered by the Hertzian Approach. The pressure distribution assumed by Hertz is a semi-ellipsoid normal pressure curve exerting pressure over both the surfaces in contact. Hertzian theory though computationally inexpensive, is based upon assumptions which are tended to get violated while estimating actual contact parameters during rail-wheel contact. For example, bodies in contact may tend to show plastic behavior and laws of plastic ratcheting will come into the play. That is why, FEA and other numerical integration techniques involving simple direct formulation into rail–wheel contact problems are favored by railway engineers and researchers to verify their results by equating them to their actual life determined over the past years. Murat et. al. and Yaylaci et. al. suggests that FEA can be an efficient alternative method to the analytical solutions. The FE approach is further categorized into assumption of elastic material properties or elasto-plastic material properties for the rail. Sladowsky et. al. assumed elastic rail and wheel material and solved the contact problem for static and quasi-static loading to determine distribution of contact zone for various rail and wheel geometries. Zhao et. al. studied the problem for both normal and tangential contacts in elastic rail and found good agreement between the FE results and analytical Hertzian approach. Tigdemir et. al. modeled wheel-snow interaction using Explicit FEA package. Assumption of elastic rail material properties gives unrealistically high stresses and eventually may lead to errors in calculation of fatigue life of the rail and wheel. For this reason, authors have looked into the prospect of assuming elasto-plastic rail material. Johansson et. al. simulated dynamic rail-wheel interaction for a single wheel pass assuming plastic material properties in rail to study the effect of vehicle running conditions. Kubin et. al. developed a 2-D FE model with elasto-plastic rail properties which accounts for roughness of the contact surfaces. Toumi et. al. studied 3-D FE frictional wheel-rail rolling contact in an elasto-plastic rail for explicit, implicit quasi-static and implicit moderate energy dissipation schemes. While authors have studied the problem of rail-wheel contact in detail, research on the combination of thermal and mechanical load and its effect on contact characteristics has

been limited. Wu et. al. developed a 2-D FE model to study the thermo-elasto-plastic deformation in material during sliding of wheel. K D Vo et. al. coupled thermal and mechanical loads in a 3-D FE model and evaluated the contribution of thermal effects and plasticity on contact characteristics. The studies however had the following limitations: 1) The material properties were considered independent of the temperature which is not the case for wheel-rail material, 2) Presence of wheel is simplified by means of a moving heat load over the rail surface which only establish full-slip contact and thus partial-slip conditions were ignored. Based on this knowledge, it can be understood that a new method for estimation of rail-wheel simulation under a combination of thermal and mechanical load is required.

The current study offers advantage of evaluating contact characteristics on the rail surface under the combined effect of thermal and mechanical loading while considering temperature dependent elastic and elasto-plastic material properties. The 3-D dynamic model will help in establishing variation in contact parameters when vehicle is in running conditions. The proposed research further aims at comparing the effect of elastic and elasto-plastic material behavior on the rail-wheel contact conditions. The contact parameters thus obtained as a result of assuming elasto-plastic material behavior will then be used to determine fatigue life of rail having an existing initial crack under the combined effect of thermo-mechanical loading.

FINITE ELEMENT METHOD

A 3-D elastic–plastic FE model is used in the present study to reproduce the motion of wheel over the rail. In the present study, rail-wheel contact is considered flexible-to-flexible as both surfaces are deformable. The wheel and rail geometry considered are 920 mm and UIC 60 as per standard used by Freight wagons and tracks respectively in Indian Railways as shown in Figure 1.
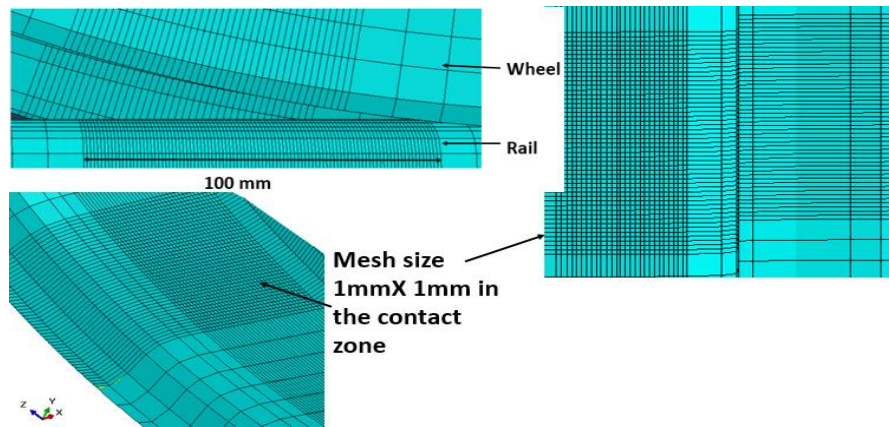
Figure 1 Meshed model of rail and wheel.

The geometries should be assembled carefully in the *Assembly* module such that the wheel is resting vertically on the rail. The contact characteristics are obliged to change in accordance with the relative position of wheel and rail. The problem of Rail-wheel interaction in FEA on account of variation of contact forces, is significantly non-linear in nature and thus is highly dependent on the mesh size and shape in the contact region. The model is meshed with 351,732 C3D8T brick elements which are capable to calculate trilinear displacement and temperature in a coupled temperature-displacement analysis. The size of the mesh in the contact region is taken to be 1mm*1mm to systematize results for all the simulation cases. Appropriate mesh convergence analysis is performed to suggest that the results in the contact region are estimated under minimal influence of mesh size.

Kinematic contact constraint which actively predicts and corrects the contact characteristics after every time increment is created between the contacting surfaces. The coefficient of friction between the interacting surfaces is assumed to be 0.3. The wheel bore surface is connected to the *Inertial Mass* of the wagon by means of a *Tied Constraint*. An initial rotation and translation which is kept constant over the simulation time is further applied on the wheel. Simulation time was kept 0.1 second in due accordance with Courant stability condition. Keeping time step small in an *Explicit* analysis assures convergence and inclusion of all the vibration modes in the FEA result. In contrast, analytical estimation by means of Hertzian Approach ignores the vibration of the structure and the continua excited by the motion of the

wheel on the rail. Therefore, for the purpose of correct comparison between the analytical and FEA results, rail should be supported by a rigid foundation by means of *Rigid Body constraint*. The total load acting on the rail consists of mass of the wheel which is 1000 kg and a fragment of the vehicle mass. The wheel is assumed to be of elastic in nature and the rail surface is modeled with elasto-plastic material behavior as shown in Table 1 (Srivastava et. al., 2017). The properties used to exhibit thermal behavior of the rail steel is shown in Table 2.

Table 1 Mechanical Elastic and Elasto-plastic properties of Rail and Wheel Steel

Temperature (^{o}C)	Young's Modulus (MPa)	Poisson's ratio	Yield Strength (MPa)	Kinematic Hardness Parameter, C_1 (MPa)	γ_1
20	180	0.2841	540	20800	26
100	180	0.2865	540	19600	25.4
200	180	0.2902	540	18000	24
300	175	0.2940	540	16000	27.7
400	170	0.2985	540	13900	34

Table 2 Thermal properties of Rail and Wheel Steel (Srivastava et. al., 2017)

Temperature (^{o}C)	Thermal Conductivity (W/m ^{o}C)	Coefficient of Thermal Expansion (X 10^{-6}K^{-1})	Specific Heat (J/kg ^{o}C)
20	47.1	11.72	468.6
100	47.1	12.2	490.7
200	45	12.8	527.2
300	43	13.4	565.9

QUALITATIVE HEAT TRANSFER ANALYSIS

Simulations of wheel passing over a point on the rail are performed using Abaqus CAE. When the wheel crosses the predefined point on the rail during braking, the sliding action produces high temperature on the wheel as well as the rail surface. As a consequence of this thermal load which is acting in combination with mechanical load of the vehicle, the material of rail undergoes plastic deformation and a dent remains after the first passage of the wheel. Every following passage of wheels from that point onward during the course of braking will then partly impact on a deformed surface of the rail.

SYNTHETIC LOADING SPECTRUM

In this paper, the multi-physics phenomenon concerning both mechanical and thermal analysis are coupled simultaneously to allow for estimation of life of rail. Total stress acting on the rail is a combined outcome of the thermal stresses induced in the rail due to the sliding of wheel and structural stresses originated due to the axle load on the wheel. The resultant stress produced due to the combination of thermal and mechanical loading will then be used to estimate stress intensity factor. As a part of this study, it is further assumed that a point on the rail surface will be under the effect of thermal load only until the wheel passes over it, at which point it will be under the combined effect of both thermo-structural loads. Stress intensity factor will then serve as an input to estimate fatigue crack growth. Number of cycles for a crack to grow from an initial length to a final length will be eventually determined using modified Paris Law and Generalised Frost-Dugdale approach as discussed in Appendix-I.
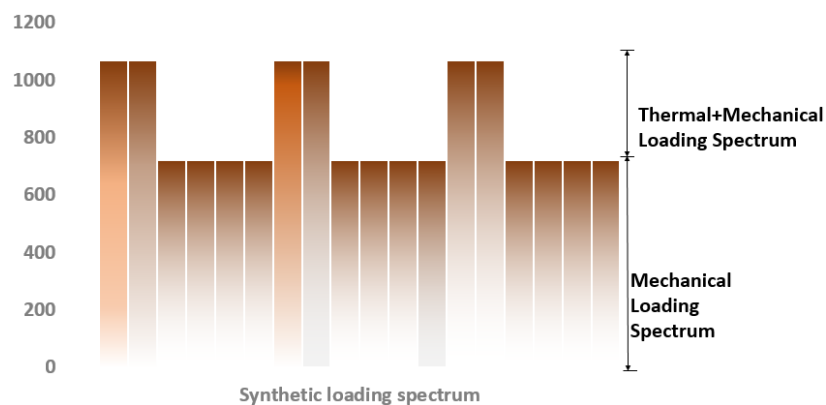
Figure 2 Synthetic Loading Spectrum

In this case, the train assumed initially running at an initial velocity brakes while entering the platform. Braking action will result in increasing sliding motion at the rail-wheel interface. Synthetic method (Peng et. al., 2012) assumes that thermal loading is acting for M cycles beginning from the instant braking is initiated as shown in Equations (1-2). Mechanical loading will act only when there is contact between the points of stress estimation on the rail and the wheel. Assuming N cycles of mechanical loading such that N<M. All the cycles in thermal loading spectrum are divided into M/N equal parts whereas in mechanical loading spectrum divided into N parts.

$$\sigma_i^{Synthetical} = \sigma_j^{Mechanical} + \sigma_k^{Thermal} \in i = k: k = (j-1)\frac{M}{N} + 1 \qquad (1)$$

$$\sigma_i^{Synthetical} = \sigma_k^{Thermal} \in i \neq k \tag{2}$$

Synthetic loading spectrum adds the thermal and mechanical stress magnitudes at same cycle while keeping the rest of the values unchanged as shown in Figure 2.

RESULTS AND DISCUSSIONS

All the FE simulations were performed using 3.2 GHz Intel® Core TM I78700 workstations. In this section, results from variation of load using Hertzian approach and FEA approach are discussed. The vertical normal force on the wheel due to the axle is varied from 70 kN to 130 kN to envelope the variation of loads carried by all types of passenger and freight wagons used by Indian Railways. The contact pressure and contact area are observed to be increasing with an increase in the axle load of the vehicle as shown in Figure 3(a) and Figure 3(b). For a *Dynamic Explicit* analysis, the appropriateness of the simulation response can be evaluated by use of *Energy Balance* Equation 3.

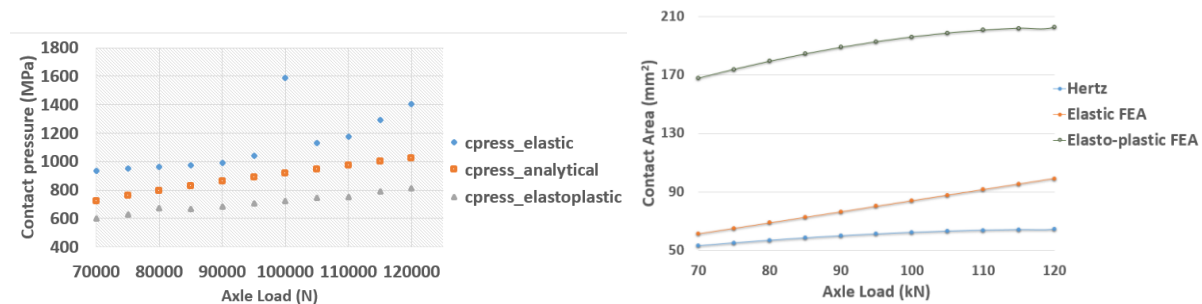$$ALLWK=ALLIE+ALLKE+ALLVD \tag{3}$$

Figure 3 Variation of a) contact pressure b) contact area at rail-wheel interface with axle load

The plots comparing external work of applied forces for the whole model and algebraic sum of the Internal Energy, Kinetic Energy and Viscous Dissipation Energy of the model for elastic material response can be seen in Figure 4. The closeness of the two curves throughout simulation time suggests that the energy equilibrium is satisfied. It is observed that results from elasto-plastic FEA differs notably from Hertzian or elastic FEA formulations and agrees with the data from field trials and experiments. A valid explanation for this behavior is the increase in contact area size at the rail-wheel interface while using the elasto-plastic FEA. The contact area is no longer elliptical as shown in Figure 5 and symmetric as found during

Hertzian or elastic FEA approach, instead has a conicity in the rolling direction. Distribution of Contact Pressure and Von Mises stress on the rail surface can be seen in Figure 6(a) and Figure 6(b) respectively. Variation of contact area over the course of simulation of wheel on the rail assuming elastic material properties for both rail and wheel is shown in Figure 7. It can be seen that the contact area keeps on varying throughout the simulated motion of the wheel owing to the non-linearity in contact and asymmetric wheel profile geometry. These continuous fluctuations in the contact simulations are termed as *Contact Chattering* and are largely observed in the coarse mesh region. Contact pressure and contact area results from various approaches used in this paper are found in agreement with Toumi et. al. In addition to it, distribution of plastic strain across the transverse and longitudinal directions of rolling can be seen in Figure 8(a) and Figure 8(b) respectively.

INFLUENCE OF TEMPERATURE

Heating of the rail material leads to thermo-mechanical fatigue and generation of white brittle etching layer which increases the possibility of crack initiations and growth. Therefore, an indirect coupled thermo-elasto-plastic FEA approach is employed to evaluate the effect of motion of the wheel on the contact pressure and temperature of the rail. This approach is applied in two stages: firstly, the estimation of temperature distribution profile on the rail surface during the simulated movement of wheel over the rail surface, and secondly combining the thermal load on the rail surface with the structural load to determine displacement, strains and stress field on the rail surface. The maximum temperature on the rail surface as shown in Figure 9 due to the sliding motion of wheel is found to be 227°C which is significantly lower than the critical temperature of steel (approximately 730°C) required for phase transformation. Free convection to environment is assumed to model natural convection of air using standard correlations to simulate heat dissipation from the rail surface.

FATIGUE LIFE ESTIMATION

Modified Paris law suggests that number of cycles required for a crack to grow is a function of initial crack length. As a part of this study, various initial crack sizes are taken to study the

life of rails near platforms and stations in Indian Railways. A 24 coach Indian Railways passenger train as shown in Figure 10 consist of 96 wheels for each rail. Assuming each wheel imparts uniform heat to the rail surface while braking, a total of 96 coupled thermo-structural loading cycles will be experienced by a point on the rail for every passenger train coming to a halt at the junction. In this article, we have considered the number of trains terminating and halting at New Delhi Railway Station, having 16 platforms where an average of 225 trains terminates and stops on a daily basis. It is further assumed that each platform invites same number of trains and each train has same number of coaches. Standard calculations imply that each rail surface may thus live through approximately 500,000 loading cycles of thermal and coupled thermo-structural loads every year. Initial flaws are typically categorized on the basis of their length as: i) micro-cracks (less than 0.5mm) ii) small cracks (size varying from 1mm to 2 mm) and iii) large cracks (size greater than 2mm). Variation of final crack size as a function of initial crack length and number of loading cycles can be seen in Figure 11(a), Figure 11(b) and Figure 11(c) respectively.
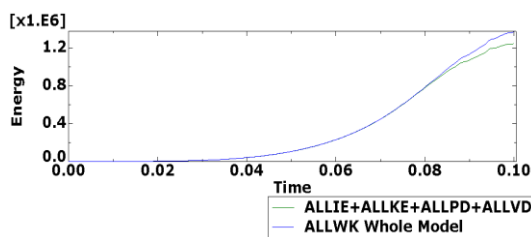

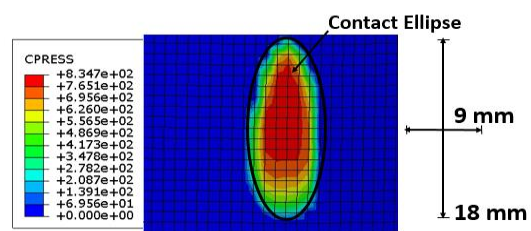**Figure 4** Energy balance plots for the whole model for elastic material behavior.

Figure 5 Shape and size of contact patch assuming elasto-plastic rail material properties.
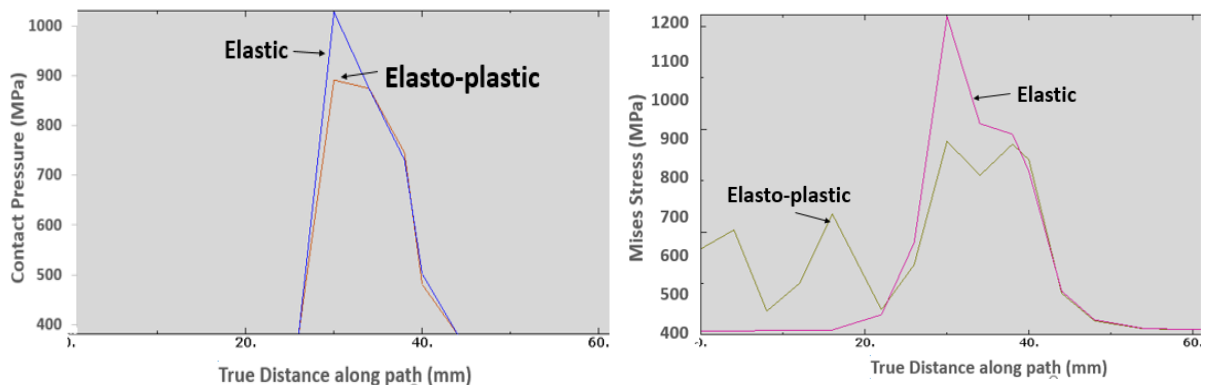

Figure 6 Variation of a) contact pressure b) Stress distribution along longitudinal direction of

10

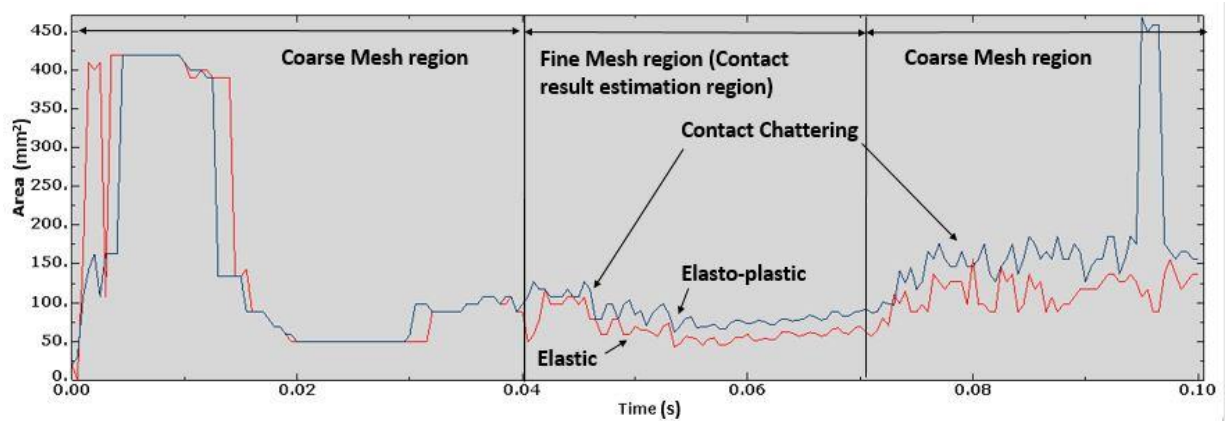travel for elastic and elasto-plastic materials

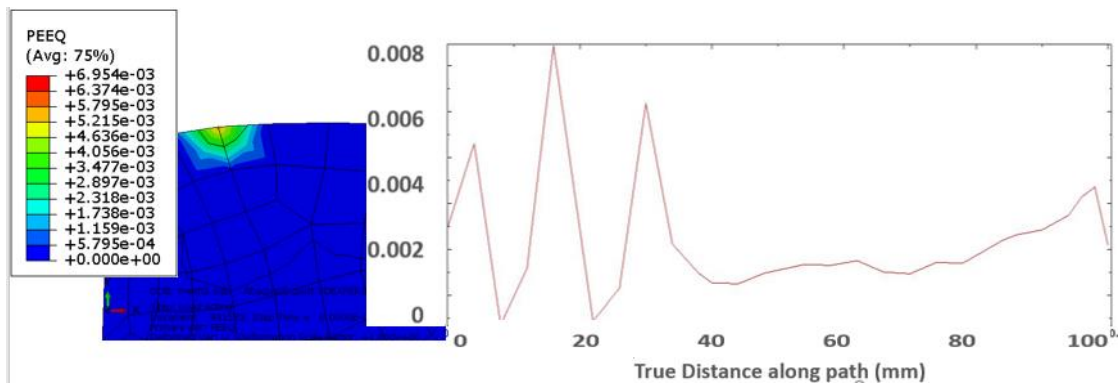**Figure 7** Variation of contact area at rail-wheel interface during the course of simulation

Figure 8 Equivalent plastic strain distribution on rail across a) cross-section of rail b)
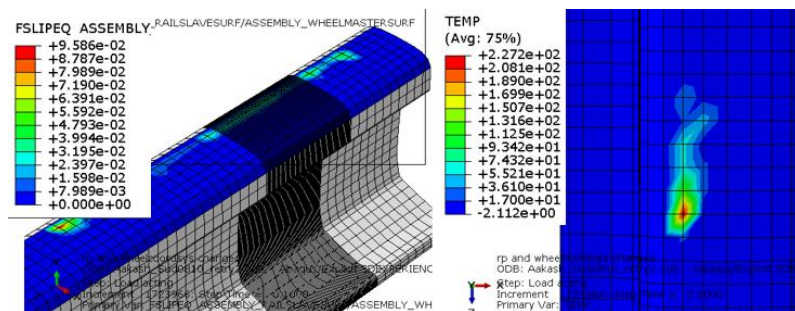
longitudinal direction of travel

Figure 9 Temperature distribution on the rail during the sliding motion of wheel
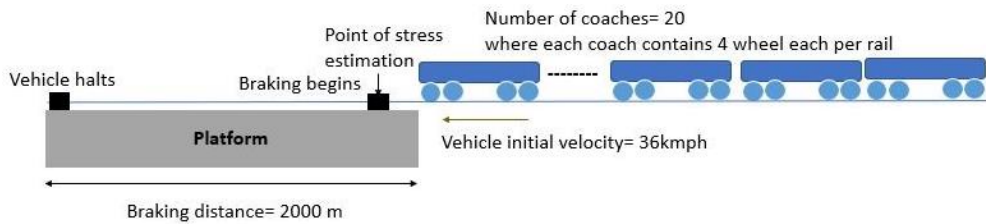
11

Figure 10 Schematic sketch of the passage of bogie over a point on the rail

CONCLUSION

It is observed that the normal contact solution considering elastic material properties in FEA model is in a good agreement with the Hertzian approach. It can also be seen that while considering elasto-plastic material properties in rail, both Von Mises stress and contact pressure reduced significantly. The elasto-plastic contact pressure is 1.25 and 1.75 times lesser than the analytical Hertzian and Elastic FEA approach respectively. The contact area is found to be larger and shape of contact patch in elasto-plastic FEA is not uniformly elliptical as determined with elastic FEA and Hertzian approach, instead has a conicity in the direction of travel. An indirect coupled thermo-mechanical approach is used to study the effect of temperature on the existing crack growth during the sliding motion of the wheel during braking. The analysis revealed that major cracks having initial length more than 2mm are very critical and require frequent attention and maintenance. It is to be noted here that simulations in this article are performed considering a uniform deceleration rate of 0.5 m/s^2 of vehicle. An increase in rate of deceleration can further increase the temperature on the rail surface and can consequently increase the rate of crack growth. The presented model discusses the impact of considering elasto-plastic material properties for assessing contact parameters at the rail-wheel interface. It further highlights the importance of temperature generated on the rail surface during the sliding motion of the wheel and its effect on the growth of cracks present on the contact surface.
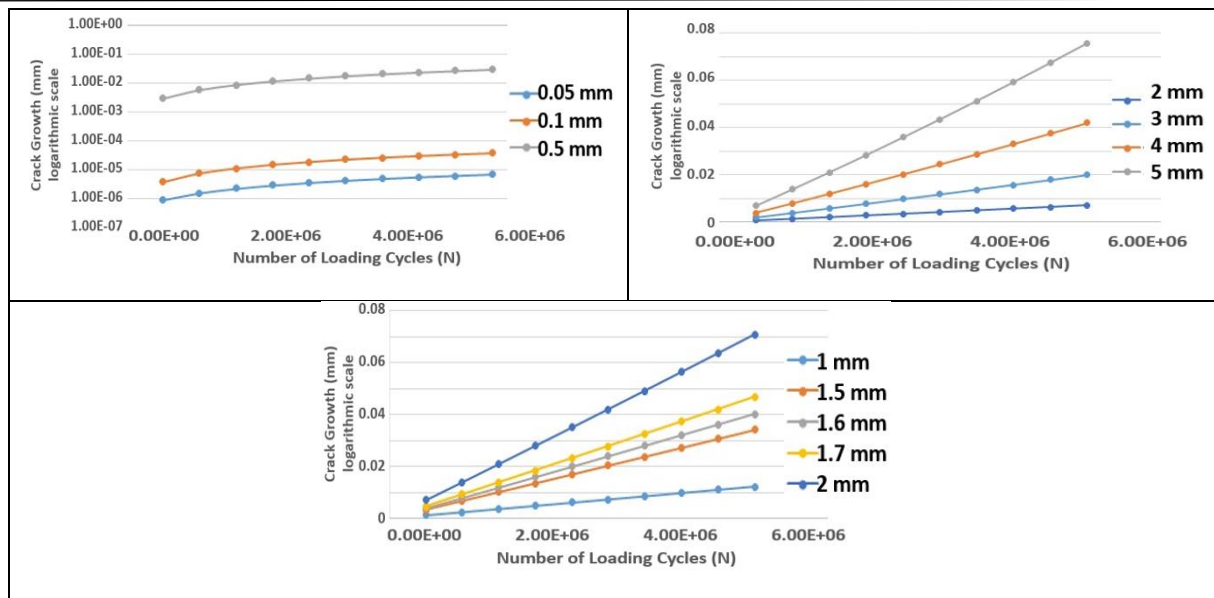
Figure 11 Comparison of a) micro b) small c) macro/large scale crack growth

REFERENCES

Taciroglu, M. V., Karasahin, M., Tigdemir, M. & Isiker, H., 2020. Fractal analysis of high speed rail geometry data: A case study of Ankara-Eskisehir high speed rail. Measurement.165: 108120-108134.

Ayasse, J. B., & Chollet, H., 2005. Determination of the wheel rail contact patch in semi-Hertzian conditions. Vehicle System Dynamics, 43(3), 161–172.

Piotrowski, J., & Chollet, H., 2005. Wheel-rail contact models for vehicle system dynamics including multi-point contact. Vehicle System Dynamics, 43(6–7), 455–483.

Kalker J. J. & Johnson K. L., 1993. Three-dimensional elastic bodies in rolling contact. Solid mechanics and its applications, Springer-Science+ Business Media B.V.

Murat, Y., & Mehmet, A., 2020. Finite element modeling of contact between an elastic layer and two elastic quarter planes. Computers and Concrete, 26(2), 107–114.

Murat, Y., Terzi, C. & Mehmet, A., 2019. Numerical analysis of the receding contact problem of two bonded layers resting on an elastic half plane. Structural Engineering and Mechanics, 72(6), 775–783.

Sladkowski, A., & Sitarz, M. 2005. Analysis of wheel-rail interaction using FE software. Wear,

258(7–8), 1217–1223.

Zhao, X., & Li, Z. 2011. The solution of frictional wheel-rail rolling contact with a 3D transient finite element model: Validation and error analysis. Wear, 271(1–2), 444–452.

Mesut, T., Mahyar, J. & Mehmet, C. B., 2018. Numerical modeling of wheel on the snow. International Journal of Engineering and Applied Sciences, 10(2), 64–72.

Johansson, A., Pålsson, B., Ekh, M., Nielsen, J. C. O., Ander, M. K. A., Brouzoulis, J. & Kassa, E., 2011. Simulation of wheel-rail contact and damage in switches & crossings. Wear, 271(1–2), 472–481.

Kubin, W. K., Pletz, M., Daves, W. & Scheriau, S., 2013. A new roughness parameter to evaluate the near-surface deformation in dry rolling/sliding contact. Tribology International, 67, 132–139.

Toumi, M., Chollet, H., & Yin, H. 2016. Finite element analysis of the frictional wheel-rail rolling contact using explicit and implicit methods. Wear, 366–367, 157–166.

Wu, L., Wen, Z., Li, W. & Jin, X., 2011. Thermo-elastic-plastic finite element analysis of wheel/rail sliding contact. Wear, 271(1–2), 437–443.

Vo, K. D., Tieu, A. K., Zhu, H. T. & Kosasih, P. B., 2015. The influence of high temperature due to high adhesion condition on rail damage. Wear, 330-33, 571–580.

Srivastava, J. P., Sarkar, P. K., Meesala, V. R. K. & Ranjan, V., 2017. Rolling contact fatigue life of rail for different slip conditions. Latin American Journal of Solids and Structures, 14(12), 2243–2264.

Peng, D., Jones, R., Constable, T., Lingamanaik, S. N. & Chen, B. K., 2012. The tool for assessing the damage tolerance of railway wheel under service conditions. Theoretical and Applied Fracture Mechanics, 57(1), 1–13.

APPENDIX-1

Generalized Frost Dugdale approach suggests that stress intensity factor, K and crack growth can be given by:

$$\Delta K = K_{max} - K_{min} = F\sqrt{\pi a}(\sigma_{max} - \sigma_{min}) \qquad (4)$$

where ΔK is the change on stress intensity factor, a_i is the initial crack length and F is the

finite element correction factor given by:

$$F = F_e + (F_s - F_e)e^{-\alpha_d\left(\frac{a}{\rho}\right)} \tag{5}$$

where F_e and F_s are Stress Intensity Boundary Correction Factor and

$$F_e = \left[M_1 + M_2\left(\frac{a}{t}\right)^2 + M_3\left(\frac{a}{t}\right)^4\right]gf_\phi f_w \tag{6}$$

$$M_1 = 1 \qquad M_2 = \frac{0.05}{0.11+(a/c^*)^{1.5}} \qquad M_3 = \frac{0.29}{(0.23+(a/c^*)^{1.5}} \tag{7}$$

where M_1, M_2, M_3 are Applied Bending Moment

Curve Fitting function, $g = 1 - \left[\frac{\left(\frac{a}{t}\right)^4(2.6-2\left(\frac{a}{t}\right))^{t/2}}{(1+4(a/c^*)}\right]\cos\phi \tag{8}$

Angular function from elliptical crack solution, $f_\phi = \left[\left(\frac{a}{c^*}\right)^2\cos^2\phi + \sin^2\phi\right]^{0.25} \tag{9}$

Modified Paris law suggests that,

$$\frac{da}{dN} = C.a^{(1-\epsilon/2)}.(\Delta K^\eta.K_{max}^{1-\eta})^\epsilon = A.(\Delta\sigma)^\eta(\pi a)^{\eta/2}.\alpha^\eta \tag{10}$$

where the material properties assumed for crack growth rate are ε=3, η=1 and C=3.38E-12 m/cycle. Value of constant A also varies with initial crack size as:

$$A = C.a^{\left(1-\frac{\epsilon}{2}\right)} \tag{11}$$

Integrating the above equation, we get the analytical formula for calculating number of loading cycles required for a crack to grow from an initial size of a_i to a final size of a_f

$$N_f = \int_0^{N_f} dN = \int_{a_i}^{a_f} \frac{da}{A(\Delta\sigma)^\eta(\pi a)^{\eta/2}\alpha^\eta} = \frac{1}{A(\Delta\sigma)^\eta(\pi)^{\eta/2}}\int_{a_i}^{a_f} \frac{da}{(\alpha)^\eta(a)^{\eta/2}} = \frac{1}{A(\Delta\sigma)^\eta(\pi)^{\eta/2}(\alpha)^\eta}\int_{a_i}^{a_f} \frac{da}{(a)^{\eta/2}}$$

$$N_f = \frac{a_f^{\frac{-\eta}{2}+1}-a_i^{\frac{-\eta}{2}+1}}{\left(\left(-\frac{\eta}{2}+1\right)A(\Delta\sigma)^\eta(\pi)^{\frac{\eta}{2}}(\alpha^\eta)\right)} \tag{13}$$